One-dimensional pnictogen allotropes inside single-wall carbon nanotubes

*Martin Hart,[1] Ji Chen,[2] Angelos Michaelides,[3] Andrea Sella,[1] Milo S. P. Shaffer[4] and Christoph G. Salzmann[*1]*

[1] Department of Chemistry, University College London, 20 Gordon Street, London, WC1H 0AJ, United Kingdom

[2] School of Physics, Peking University, Beijing 100871, P. R. China

[3] Thomas Young Centre, Department of Physics and Astronomy, and London Centre for Nanotechnology, University College London, Gower Street, London, WC1E 6BT, United Kingdom

[4] Departments of Chemistry and Materials, Imperial College London, Imperial College Road, London, SW7 2AZ, United Kingdom

E-mail: c.salzmann@ucl.ac.uk

ABSTRACT

The discovery of phosphorene, a single layer of black phosphorus, has accelerated the investigation of pnictogen nanomaterials, leading to the recent identification of arsenene and antimonene. These two-dimensional nanomaterials display physical properties superior to graphene for some applications. Recently, single-wall carbon nanotubes (SWCNTs) have been filled with P_4 molecules from the melt and As_4 molecules from the vapor phase. Confined within SWCNTs, polymerization reactions yielded new one-dimensional pnictogen allotropes. Here, we show using high-resolution electron microscopy that such nanostructures can also be observed upon filling SWCNTs from the vapor phase using red phosphorus as the source material. Using larger diameter SWCNTs, the vapor phase favors the formation of double-stranded phosphorus zig-zag ladders observed here for the first time. Overall, however, SWCNTs were generally found to fill more efficiently with liquid phosphorus; substantial decreases in the filling yields were observed for both phosphorus and arsenic filling of narrow SWCNTs using the vapor route. Attempts to extend the pnitogen series, using molten antimony gave very low filling yields. However, the antimony zig-zag ladder was observed on two occasions suggesting that this structural motif dominates across the pnictogens. Computational predictions of the encapsulation energies of the various pnictogen nanostructures are consistent with the observed experimental trends and band gap calculations predict that the single-stranded zig-zag chains of all investigated pnictogens are fully metallic. Using SWCNTs with diameters greater than 1.5 nm displayed a plethora of complex new phosphorus nanostructures which highlights an exciting new avenue for future work in this area.

INTRODUCTION

The pnictogen group of chemical elements derives its name from the Ancient Greek word for 'choking', referring to the suppression of oxidation processes in the presence of nitrogen gas.[1] The physical and chemical properties of the pnictogens are remarkably diverse starting with the colorless dinitrogen gas, across phosphorus, arsenic and antimony, to the silvery and shiny metal bismuth.

The recent discovery of phosphorene, a single sheet of black phosphorus with a tunable band gap,[2-5] has sparked a flurry of excitement in nanomaterials based on these main group elements and a wide range of future applications, for example, in electronics, optoelectronics, sensing and thermoelectrics.[2-3, 6-10] The bulk allotropes of phosphorus include white phosphorus, highly reactive tetrahedral P_4 molecules that pack in three different polymorphs at ambient pressure,[11-12] amorphous red phosphorus,[13-14] fibrous phosphorus,[15-16] phosphorus nanorods,[17] as well as two layered structures, Hittorf's violet phosphorus[18-19] and black phosphorus,[13, 20] the latter being the most stable allotrope at ambient pressure.[21] Recently, a new 'blue' allotrope has been grown on gold substrates using molecular beam epitaxial growth,[22] and a 'green' allotrope has been predicted computationally.[23]

Gray arsenic (α-As) is the most stable allotrope at ambient conditions and consists of layers of puckered hexagons in a rhombohedral crystal structure.[24] The black allotrope (β-As) is metastable with an orthorhombic layered crystal structure similar to that of black phosphorus.[25] Amorphous arsenic, with a wide range of different densities, has also been identified.[24, 26] Analogous to white phosphorus, yellow arsenic (γ-As) consists of tetrahedral As_4 molecules.[27] However, due to its extreme sensitivity towards light and X-rays, which trigger the conversion to gray arsenic, no crystallographic data is available for γ-As.[28] In addition to the bulk allotropes,

gas-phase clusters in size up to As[5] have been identified experimentally.[29] Arsenene, the arsenic equivalent of phosphorene, displays a large bandgap[30-31] which, combined with a low thermal conductivity, makes it a highly desirable material for thermoelectric applications.[32] Other electronic, optoelectronic, spintronic and sensing applications are also envisaged.[10] Experimentally, arsenene can be prepared using plasma-assisted deposition,[33] aqueous shear exfoliation[34] and ultrasonication of gray arsenic in appropriate solvents.[35-36]

The stable gray allotrope of antimony is isostructural with gray arsenic and this pnictogen also displays the analogous metastable black allotrope.[10] By contrast, tetrahedral Sb[4] molecules appear to only be stable in the gas phase.[37-38] However, an amorphous and highly metastable 'explosive' antimony allotrope exists.[39-40] Antimonene has recently been added to the family of pnictogen nanomaterials using mechanical exfoliation,[41] liquid-phase exfoliation[42] and epitaxial growth.[43-44]

Carbon nanotubes have been used as inert molds to prepare new one-dimensional allotropes of a range of elements including carbon in its various forms,[45-47] iodine,[48] sulphur,[49] selenium[50], tellurium,[51] as well as the two pnictogens phosphorus[52-53] and arsenic.[54] In the case of phosphorus, fibrous chains with alternating P[8] and P[2] units have been identified inside large-diameter multi-wall carbon nanotubes.[52] Single-stranded phosphorus zig-zag chains have been prepared in narrow single-wall carbon nanotubes (SWCNTs) by polymerizing encapsulated chains of P[4] molecules.[53] The formation of the zig-zag chain can be regarded as the first step from white to red phosphorus, and consequently, this one-dimensional allotrope of phosphorus has been named 'pink' phosphorus.[55] The single-stranded zig-zag chain has also recently been observed for arsenic inside SWCNTs which also forms double-stranded zig-zag ladders.[54] Carbon nanotubes also provide the environment for stabilizing the highly reactive P[4] and As[4] molecules against the infamous spontaneous combustion with atmospheric oxygen to give the corresponding oxides.[53-54] Filling

carbon nanotubes with antimony has been attempted as part of the arc-discharge preparation process;[56] however, the atomic structure of the filling material was resolved.

Here, we investigate and explore a range of questions related to the formation of one-dimensional pnictogens inside SWCNTs. Specifically, we explore (i) the filling with phosphorus from the vapor phase using red phosphorus as the source material, (ii) the existence of the double-stranded zig-zag chain of phosphorus, which has previously been observed for arsenic,[54] (iii) the dependence of filling yields and structures of the pnictogens on the diameters of the SWCNTs, and (iv) the filling of SWCNTs with antimony from the melt. Furthermore, we present a complete set of inclusion and band-gap energies of the encapsulated pnictogens using density functional theory (DFT).

EXPERIMENTAL SECTION

Purification and opening of SWCNTs

Tuball SWCNTs were purchased from OCSiAl in raw powder form and purified with steam at 900°C for 5 hours.[57] A second heat treatment in air at 450°C for 30 minutes ensured the opening of the SWCNT tips. Subsequently, the SWCNTs were refluxed in 6 M HCl for 2 hours and washed on a filter membrane with an excess of water. Finally, the sample was dried in an oven overnight at 60°C. HiPCO SWCNTs were purchased from Nanointegris Inc. in ethanol-wet cake form. The supplied material was dried at 100°C and 10^{-2} mbar for 4 days, and then tip-opened by heating to 400°C in air. CoMoCAT SWCNTs were purchased from Sigma Aldrich in powder form and tip-opened by heating to 400°C in air.

Filling experiments with molten white phosphorus[53]

Caution: White phosphorus is volatile, extremely toxic and, especially after sublimation, pyrophoric. Extreme care should be taken when conducting experiments of this type. 50 mg of the SWCNTs were heated to 200°C at 10^{-6} mbar and transferred into a glove box under vacuum. Crude white phosphorus was purified by vacuum sublimation onto a liquid nitrogen-cooled probe in a Schlenk flask attached to a dual manifold Schlenk line. In a glove box, the sublimation probe was transferred immediately to a second Schlenk flask loaded with the SWCNTs and a Teflon-coated magnetic stirrer. Back on the Schlenk line, warm water was poured into the sublimation probe to melt the white phosphorus onto the SWCNTs. The black mixture was stirred at 50°C under nitrogen for one hour. Subsequently, the sublimation probe water was poured out of the probe, and after rinsing with a little acetone, was replaced with liquid nitrogen to collect excess white phosphorus subliming from the SWCNTs. The probe was removed in the glove box and set aside for storage. The Schlenk flask was returned to the Schlenk line and the filled SWCNTs were suspended in 125 mL deionized water and sonicated for 5 minutes to help disperse the mixture. Compressed air was then gently bubbled through the stirred suspension for two days using a needle to oxidize any excess white phosphorus. The sample was filtered in air on a Hirsch funnel using glass-fiber filter paper, washed with deionized water and dried in a desiccator. Caution: if the air oxidation step is shortened or omitted, the nanotubes can be pyrophoric and ignite spontaneously on the filter.

Filling experiments with phosphorus from the vapor phase

20 mg SWCNTs and 20 mg red phosphorus were ground in an agate mortar and pestle for 5 minutes to create a homogenous mixture. The mixture was then transferred to a 200 mm long quartz ampoule which was pumped down to 10^{-6} mbar, heated to 200°C at 7°C min^{-1} and held for 2 hours. The ampoule was then sealed under dynamic vacuum, heated in a tube furnace to 500°C

at 10°C min^{-1} and held for 12 hours with the sample end in the center of the furnace. After cooling, the ampoule was rotated by 180° and the sample reheated as before to sublime the white phosphorus along the length of the ampoule. This step was preformed three times. The fourth and last heat treatment sublimed the white phosphorus onto the SWCNTs located at the cool end of the ampoule. After recovering the sample from the ampoule in a glove box, the sample was transferred to a Schlenk flask as in Section 2.2, suspended in water and the excess white phosphorus removed by bubbling air through the suspension. The nanotubes were recovered by filtration onto glass-fiber paper on a Hirsch funnel.

Filling experiments with arsenic from the vapor phase[54]

Caution: Even small amounts of arsenic are highly toxic. 20 mg SWCNTs and 20 mg gray arsenic were ground for 5 minutes using an agate pestle and mortar to create a homogenous mixture. The mixture was then placed in a 200 mm long quartz ampoule which was pumped down to 10^{-6} mbar, heated to 200°C at 7°C min^{-1} and held for 2 hours. The ampoule was sealed under dynamic vacuum, heated in a tube furnace to 615°C at 10°C min^{-1} and held for 12 hours with the sample end in the center of the furnace. The ampoule was reheated three more times, each time rotating the ampoule by 180° to sublime the arsenic along the ampoule. The fourth and last heat treatment sublimed the arsenic onto the SWCNTs located at the cool end of the ampoule. After recovering the sample from the ampoule, excess arsenic was removed by stirring in 100 mL 0.5 M nitric acid solution for 4 hours followed by filtration and washing with water.

Filling experiments with molten antimony

30 mg SWCNTs and 30 mg gray antimony were ground for 5 minutes in an agate pestle and mortar to create a homogenous mixture. The mixture was then placed in a 200 mm long quartz ampoule

which was pumped down to 10^{-6} mbar, heated to 200°C at 7°C min^{-1} and held for 2 hours. The ampoule was sealed under dynamic vacuum, heated in a muffle furnace to 700°C at 10°C min^{-1} and held for 66.5 hours. After recovering the sample from the ampoule, excess antimony was removed by stirring in 150 mL 1 M nitric acid solution for 4 hours followed by filtration and washing with water.

High-resolution transmission electron microscopy (HRTEM)

The filled SWCNTs were prepared for HRTEM by sonication in absolute ethanol for 1 minute and then dropping the dispersions onto lacey carbon Agar 300 mesh copper grids. HRTEM was conducted using a FEI Titan 80/300 STEM/TEM instrument fitted with a Cs (image) corrector. The microscope was operated at 80 kV to reduce electron beam damage to the samples. The image corrector was necessary to image the structure of the SWCNTs by reducing the effects of spherical aberrations. All images were taken with the image corrector corrected to at least 18 mrad. Simulated TEM images were obtained using the SimulaTEM software[58] using an accelerating voltage of 80 kV, a defocus value of –310.2719 Å and a spherical aberration constant of 0.15 mm.

X-ray photoelectron spectroscopy (XPS)

X-ray photoelectron spectroscopy of the samples on indium foil was carried out using a Thermo Scientific K-Alpha instrument with a monochromated Al Kα X-ray source and flood gun. Survey scans were obtained by accumulating three spectra with a resolution of 1 eV and pass energy of 200 eV. High-resolution scans in the P2p, As3d and Sb3d regions were obtained from the average of 10 spectra recorded with a resolution of 0.1 eV and pass energy of 50 eV. A 400 μm spot size and 50 ms dwell time was used for each scan.

Computational methods

DFT calculations were performed using the Vienna ab initio Simulation Package (VASP) where the core electrons were described with projector augmented wave (PAW) potentials.[59-60] An energy cutoff of 400 eV was used to expand the wave functions. The optB86b-vdW van der Waals inclusive exchange correlation functional was used.[61] An empirical cylindrical confining potential was implemented to simulate the confinement of carbon nanotube following the procedure used previously.[53, 62] The empirical potential has a Morse-type formula defined as $V(x) = D\,[(1 - \exp(-A\,(x - R)))^2 - 1]$ in eV, where x is the distance of a pnictogen atom to the carbon nanotube wall in Å. The various parameters are: $D = 0.125, 0.172, 0.203$, $A = 1.060, 1.052, 0.974$ and $R = 3.640, 3.565, 3.733$, respectively for P, As, and Sb. The parameters used were fitted to the DFT interaction between an X_4 molecule (X = P, As or Sb) and graphene as shown in Figure S1.

RESULTS AND DISCUSSION

Filling experiments with elemental pnictogens

To investigate the various aspects of filling SWNCTs with elemental pnictogens mentioned earlier, a range of SWCNT materials were explored with different diameters, including CoMoCat ($d < 1.0$ nm),[63] HiPCO ($d = 0.8 - 1.3$ nm),[64] and Tuball ($d > 1.5$ nm).[65] The filling yields of the pnictogens were determined using XPS (Figure 1). In all cases, peaks associated with both elemental and oxidized pnictogens were observed. The complete set of XPS spectra are provided in Figures S1 and S2. The elemental pnictogens are presumed to be protected inside the SWNCTs, while the oxidized material is the result of some residual elemental pnictogens adhering to the outside walls or the tips of the tubes, and able to react with atmospheric oxygen or with the nitric acid used for purification.
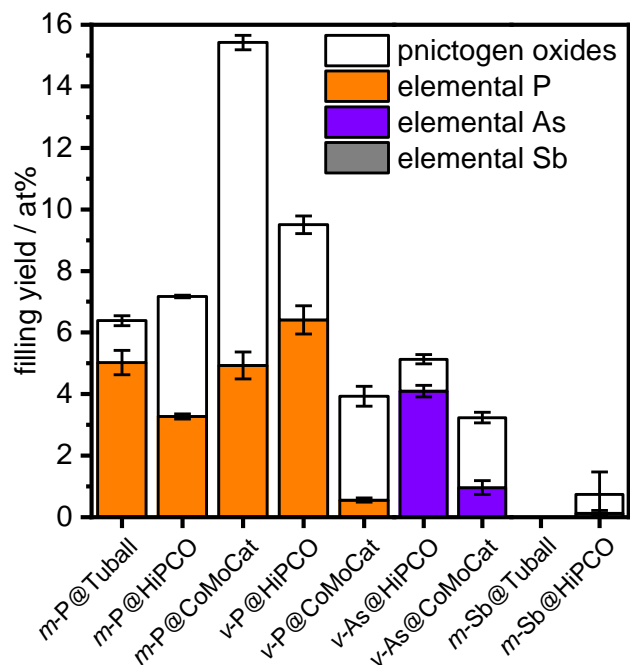
Figure 1. *Filling yields of elemental and oxidized pnictogens in various types of SWCNTs. The prefix 'm' indicates filling from the melt; 'v' denotes vapor-phase filling. The filling yields were determined by fitting the survey and high-resolution XPS spectra shown in Figure S2 and S3. The error bars were calculated by measuring at least three XPS spectra for a given sample. The filling yields of m-P@CoMoCat and v-As@HiPCO were reported in our earlier studies.[53-54]*

Some of the highest filling yields were observed for elemental phosphorus using the melt filling technique and they were found to be relatively independent of the diameter of the SWCNTs. Filling with phosphorus from the vapor phase was successful as well and gave the single highest filling yield out of all experiments in the case of HiPCO tubes. The filling yield using the smaller diameter CoMoCat tubes was considerably lower. These findings suggest that if P_4 molecules fit inside the SWCNTs, then filling from the melt is generally viable. However, the vapor filling does seem to be more effective for larger-diameter SWCNTs suggesting some limitations for the vapor condensation of P_4 molecules into small-diameter SWCNTs.

As previously reported,[54] HiPCO SWCNTs also fill well with elemental arsenic from the vapor phase, delivering comparable filling yields as obtained for phosphorus. Similar to the v-P@CoMoCat experiment, CoMoCAT SWCNTs exhibited a relatively low filling yield for elemental arsenic. Because As_4 is notoriously thermally unstable in the solid state,[66] the filling of SWCNTs with elemental arsenic from the liquid phase appears to be impossible.

Whilst an XPS signal for antimony was detected for the melt-filling experiments, the absolute filling yield of elemental antimony was too low to be quantitatively determined (nominally only 0.13 at% for m-Sb@HiPCO). Unlike molten white phosphorus, liquid antimony does not contain any molecular species.[67] The poor filling yield is likely to be due to the high surface tension of molten antimony (368 mN m^{-1})[68] which exceeds the often quoted limit[69] for filling SWCNTs of 200 mN m^{-1}. Even if Sb_4 molecules formed upon entering the SWCNTs, they would be expected to be highly unstable. For example, attempts at isolating yellow antimony on a graphite surface resulted in the growth of a complex selection of extended nanostructures around defect sites.[70]

The amounts of pnictogen oxides were found to vary substantially from sample to sample. Pnictogen oxides are expected to form as remaining external material reacts with atmospheric oxygen or nitric acid. The elemental filling material is passivated by the carbon nanotubes and by oxide 'caps' at the open ends. In line with this interpretation, the HRTEM images of the filling materials can be simulated with pure elemental filling structures, as discussed further below, and occur independently of the oxide content identified by XPS. In HRTEM, disordered structures were often observed within the open porosity of the 'entangled' agglomerates of SWCNTs; most likely, these locations are where the bulk of the pnictogen oxides are located, in addition to the open ends of SWCNTs. When phosphorus-filled SWCNTs are 'capped' with C_{60} molecules dissolved in ethanol, the internal filling is passivated independently of the oxides; in this case, the

phosphorus oxides can be removed almost quantitatively.[71] The C_{60} molecules are expected to block the oxidation of elemental phosphorus at the tips of the SWCNTs while the ethanol dissolves the external phosphorus oxides. These experiments confirm that the elemental phosphorus is located inside the SWCNTs whereas the phosphorus oxide is external as expected from the reactivity with oxygen from the atmosphere.

Microstructures of the one-dimensional pnictogen allotropes

Three different types of phosphorus and arsenic nanostructures have been identified inside the SWCNTs with HRTEM, as shown in Figure 2. These variants include lines of tetrahedral P_4 or As_4 molecules analogous to peas in a pod, the double-stranded zig-zag ladder and the single-stranded zig-zag chain. Notably, the phosphorus double-stranded zig-zag ladder is reported here for the first time whereas the other structures have been observed in our previous studies.[53-54] It is also worth mentioning that the lines of P_4 molecules and the phosphorus zig-zag chain were previously observed inside CoMoCat SWCNTs filled from the melt[53], whereas they are imaged here for the first time inside the larger diameter HiPCO SWCNTs after filling from the vapor phase.
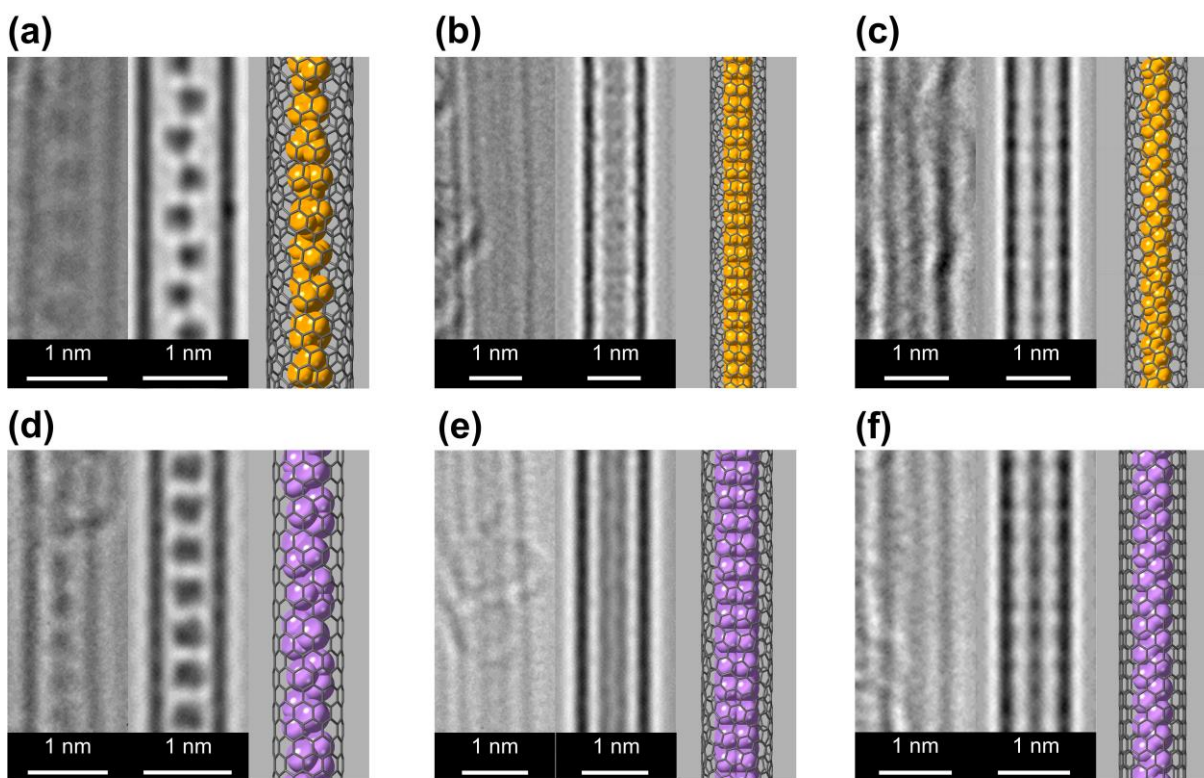
Figure 2. High-resolution transmission electron microscopy (HRTEM) images of the three different nanostructures adopted by elemental phosphorus and arsenic inside SWCNTs. Each panel shows three images including the experimental (left) and simulated micrographs (middle) as well as the corresponding DFT geometry-optimized atomistic models (right). The data for v-P@HiPCO and v-As@HiPCO are shown in (a-c) and (d-f), respectively. The imaged nanostructures include (a,d) the lines of P_4/As_4 beads, (b,e) the double-stranded zig-zag ladder and (c,f) the single-stranded zig-zag chain. The simulated micrographs were obtained by rotationally averaging the filling materials (about the center of mass for the molecular species and about the tube axis for the chain structures).

As can be seen in Figure 2, the experimental HRTEM images agree well with calculated images based on structures that were geometry-optimized with DFT. The best agreement between the experimental HRTEM images and the simulated pictures was obtained by rotationally averaging

13

the P_4 and As_4 molecules about their centers of mass, and the linear chains by rotation about the axis of the SWCNT. Similar dynamic rotations of the filling materials have been previously observed in the case of encapsulated graphene nanoribbons[47] and may be driven by the exposure to the electron beam inside the HRTEM.

The two polymerized pnictogen chain structures can be clearly distinguished on the basis of their widths. The zig-zag ladder manifests as a broad feature in HRTEM with a gap between the two parallel strands, whereas the single zig-zag chain is seen in the form of a single, narrow line. In the ladder structures, the distance between the two strands of the zig-zag chains is on average 2.38 Å for arsenic and 2.43 Å for phosphorus. As shown in Figure S4, the distance between the two strands increases slightly as the diameter of the confining SWCNT increases. This effect is seen both in the experimental data as well as for the DFT-optimized structures.

Having established the various phases present, their relative occurrence was quantified, using HRTEM, as a function of increasing SWCNT diameter and melt/vapor-phase filling. The CoMoCat and HiPCO SWCNTs used in this study displayed the expected diameter distributions, mainly in the $0.6 – 0.9$ nm and $0.9 – 1.1$ nm diameter ranges, respectively.[63-64] As shown in Figure 3(a), the narrow CoMoCat SWNCTs filled with phosphorus from the melt showed lines of P_4 molecules and zig-zag chains predominately at lower diameters and, as expected due to their larger size, zig-zag ladders at larger diameters. The larger diameter HiPCO SWCNTs, while still filling from the melt, displayed significantly different distributions of the various phosphorus nanostructures (Figure 3(b)). Due to the increased availability of larger diameter SWCNTs, the zig-zag ladder is now clearly the dominant species. Interestingly, this effect becomes even more pronounced for the vapor-filled P@HiPCO sample where the zig-zag ladder is found almost exclusively (Figure 3(c)). Compared to the filling from the melt, vapor-filling using red

phosphorus as the source material is carried out at much higher temperatures. The dominance of the zig-zag ladder in the v-P@HiPCO sample therefore suggests that increasing the temperature favors the formation of the zig-zag ladder inside the SWCNTs. As shown in Figure 3(d) and previously reported,[54] the zig-zag ladder also dominates in the case of v-As@HiPCO. However, the line of beads and the zig-zag chain are observed somewhat more frequently than for v-P@HiPCO. In summary, changing the diameter of the SWCNTs appears to have a profound effect on the structures of the encapsulated pnictogens, whereas the effect of the filling method, either from the melt or the vapor phase, seems to have a more minor effect. Of course, other factors such as the details of the chiralities of the SWCNTs, metallicity and defect concentrations may play a role as well.
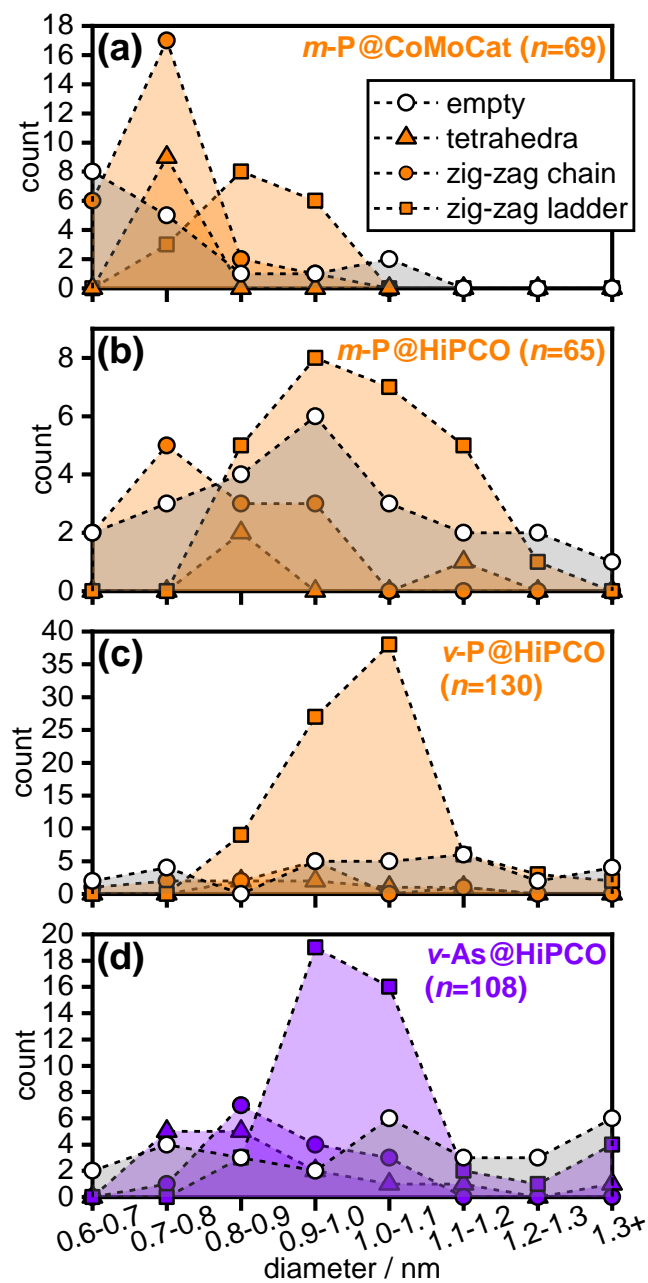
Figure 3. *Occurrences of the different pnictogen nanostructures as a function of the SWCNT diameter for (a) m-P@CoMoCat, (b) m-P@HiPCO, (c) v-P@HiPCO and (d) v-As@HiPCO. Panel (d) is reproduced from ref. 54. The total number of HRTEM observations is noted for each panel.*

Compared to the more conventionally-sized CoMoCat and HiPCO SWCNTs, large-diameter phosphorus-filled Tuball SWCNTs with diameters above 1.5 nm displayed none of the previously observed nanostructures (Figure 4). Instead, several irregularly-shaped filling materials were observed ranging from what could be hollow-shell nanostructures in Figure 4(a) to potentially two zig-zag chains or ladders arranged in a double-stranded fashion in Figure 4(c). It is noted that empty Tuball SWCNTs did not display such HRTEM features. Currently, it is not possible to make definitive assignments and much more work is clearly needed to resolve these structures including further computational studies.
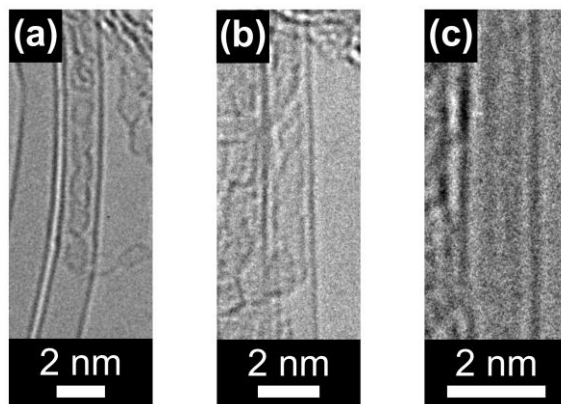

Figure 4. HRTEM images of m-P@Tuball showing encapsulated phosphorus nanostructures with irregular shapes.

Despite the low filling yield for m-Sb@HiPCO indicated by the XPS analysis (Figure 1), HRTEM showed double-stranded antimony nanostructures, on two occasions, inside the SWCNTs (Figure 5). In addition to the frequent observation of phosphorus and arsenic zig-zag ladders, this structural motif, therefore, also seems to be realized for antimony. Extensive searching for single Sb_4 molecules or the zig-zag chain was unsuccessful.
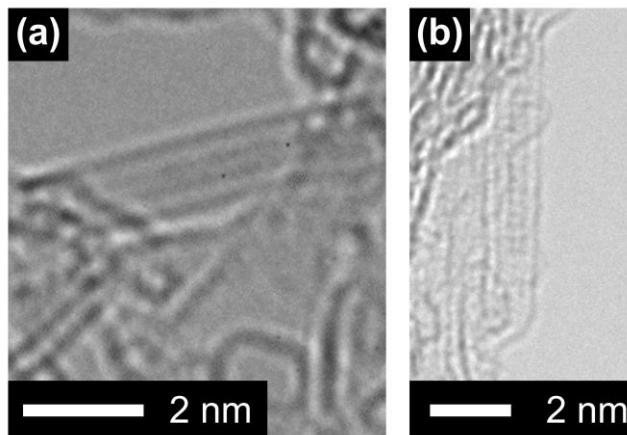
Figure 5. HRTEM images of m-Sb@HiPCO showing double-stranded structures in (a) 1.086 nm and (b) 0.963 nm diameter SWCNTs.

Computational energies and bandgaps of the one-dimensional pnictogen allotropes

The relative stabilities of the three experimentally observed one-dimensional pnictogens (Figure 6), calculated by DFT, follow the observed yields (Figure 1). The phosphorus structures are energetically the most and antimony the least stable. The lowest-energy antimony structures are zig-zag ladders at large diameters which agrees well with the observations in Figure 5. In the cases of phosphorus and arsenic, the molecular forms and the single-stranded zig-zag chain are most stable at lower diameters whereas the double-stranded zig-zag ladder becomes increasingly more stable as the confinement diameter increases. All these trends are in very good agreement with the experimental observations reported in Figure 3.
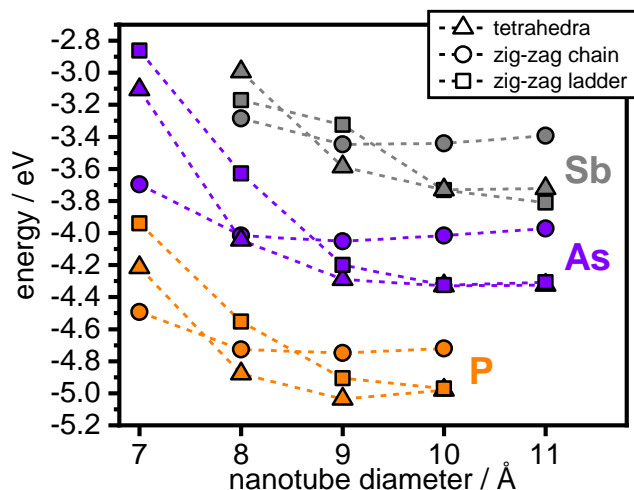
Figure 6. *DFT energies of the three one-dimensional pnictogen nanostructures as a function of the nanotube diameter and defined as the per-atom binding energy relative to the isolated pnictogen atom plus the confining energy. The numeric values of the energies separated into the contributions from binding and confining energies are given in Table S1.*

The DFT-calculated electronic densities of state of the three experimentally observed pnictogen nanostructures (Figure 7) identify a number of systematic trends. The lines of P_4 molecules display the largest band gaps that decrease down the pnictogen group for the various molecular species. Further closing of the band gaps to quite similar values for the various pnictogens is observed for the zig-zag ladders. Finally, the single-stranded zig-zag chains of all pnictogens are fully metallic with the density of states spanning across the Fermi level. Although the electronic densities of state are similar for the various pnictogen nanostructures, the features are shifted or stretched; typically away from the Fermi level for phosphorus and towards the Fermi level in the case of antimony, illustrating its general tendency towards metallic structures. The optB86b-vdW DFT functional used in this study may slightly underestimate the band gaps of the semiconducting structures. However, the transition to the metallic zig-zag chain is expected to be insensitive to the choice of functional.[54]
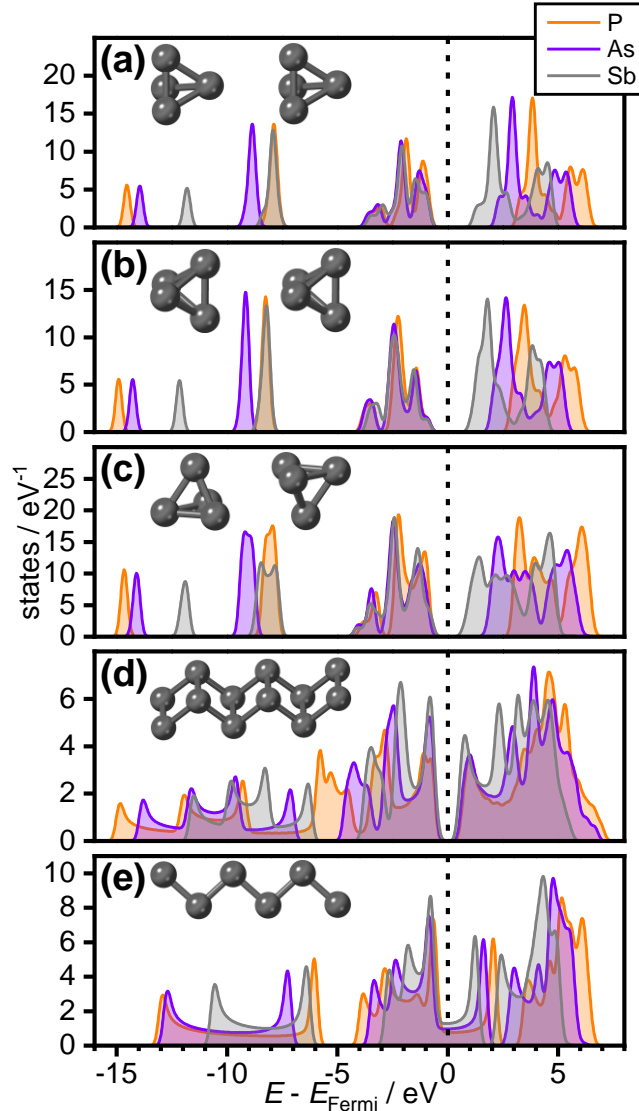
Figure 7. *Electronic densities of state of confined pnictogen nanostructures including (a) corner-to-face, (b) edge-to-edge and (c) face-to-face tetrahedra as well as (d) zig-zag ladders and (e) zig-zag chains. The Fermi level is indicated by dashed vertical lines.*

CONCLUSIONS

In summary, SWCNTs can be filled systematically with elemental phosphorus, arsenic and antimony to form one-dimensional pnictogen allotropes. The double-stranded phosphorus zig-zag ladder was observed for the first time and its relative occurrence upon filling from the melt was

found to depend on SWCNT diameter. SWCNTs were successfully filled using red phosphorus, which may be more convenient than using white phosphorus, to yield predominately the new zig-zag ladders. Whilst the filling yield from molten phosphorus showed little dependence on diameter, the vapor phase filling was more effective for the larger diameter HiPCO SWCNTs. Using red rather than white phosphorus as the starting material is certainly an improvement with respect to the safety of the filling experiments. The antimony filling yields were generally very low. However, two double-stranded structures were imaged in HRTEM suggesting that this structural motif is common across all three pnictogens. Filling SWCNTs with diameters greater than 1.5 nm with elemental phosphorus showed a range of complex new nanostructures inside the SWCNTs.

In general, the DFT-calculated energies of the various one-dimensional pnictogens were in very good agreement with the experimental findings and helped rationalizing the decreasing filling yields down the pnictogen group as well as the relative occurrences of the various nanostructures as a function of the SWCNT diameter. Furthermore, DFT calculations showed that the band gap of the confined pnictogens closes as the degree of polymerization increases and that the zig-zag chains of all three pnictogens are predicted to be fully metallic. The changes in the band gaps are most pronounced for phosphorus and much weaker for antimony reflecting the general tendency of this pnictogen towards consistent metallic behavior.

Overall, the sensitivity of the electronic behavior to structure is a very interesting aspect of the one-dimensional pnictogen allotropes. For further experimental investigation, and possibly even application, future efforts will aim to prepare the new 1D pnictogen allotropes inside insulating confinements such as boron nitride nanotubes. Furthermore, it has been pointed out that the confined phosphorus and arsenic materials could be used for making P_4 and As_4 available for chemical reactions.[53-54, 66, 72-74] Whether longer chain segments can be recovered intact from inside

the SWCNTs using appropriate solvents is another open question. A recent computational study has suggested that the one-dimensional pnictogen zig-zag chains may be stable when supported by a substrate.[75] Finally, as we have shown here, moving towards larger diameter SWCNTs opens a door to ever more complex pnictogen materials. Exploring their structures and physical properties in detail will be an exciting future challenge.

ASSOCIATED CONTENT

Supporting Information. The supporting information contains the XPS spectra used for the analysis for preparing Figure 1 in the main article as well as an analysis of the distance between the two strands of the zig-zag ladder in both the experimental HRTEM images as well as the DFT-optimized structures. A preprint version of this article has been placed on ChemRxiv.[76]

AUTHOR INFORMATION

Corresponding Author

* Email: c.salzmann@ucl.ac.uk

REFERENCES

1. Girolami, G. S., Origin of the Terms Pnictogen and Pnictide. *J. Chem. Ed.* **2009,** *86* (10), 1200.

2. Liu, H.; Neal, A. T.; Zhu, Z.; Luo, Z.; Xu, X.; Tománek, D.; Ye, P. D., Phosphorene: An Unexplored 2D Semiconductor with a High Hole Mobility. *ACS Nano* **2014,** *8* (4), 4033-4041.

3. Li, L.; Yu, Y.; Ye, G. J.; Ge, Q.; Ou, X.; Wu, H.; Feng, D.; Chen, X. H.; Zhang, Y., Black phosphorus field-effect transistors. *Nat. Nano.* **2014,** *9* (5), 372-377.

4. Koenig, S. P.; Doganov, R. A.; Schmidt, H.; Neto, A. H. C.; Özyilmaz, B., Electric field effect in ultrathin black phosphorus. *Appl. Phys. Lett.* **2014,** *104* (10), 103106.

5. Andres, C.-G.; Leonardo, V.; Elsa, P.; Joshua, O. I.; Narasimha-Acharya, K. L.; Sofya, I. B.; Dirk, J. G.; Michele, B.; Gary, A. S.; Alvarez, J. V.; Henny, W. Z.; Palacios, J. J.; Herre, S. J. v. d. Z., Isolation and characterization of few-layer black phosphorus. *2D Mater.* **2014,** *1* (2), 025001.

6. Xia, F.; Wang, H.; Jia, Y., Rediscovering black phosphorus as an anisotropic layered material for optoelectronics and electronics. *Nat. Comm.* **2014,** *5*, 4458.

7. Guo, Z.; Zhang, H.; Lu, S.; Wang, Z.; Tang, S.; Shao, J.; Sun, Z.; Xie, H.; Wang, H.; Yu, X.-F.; Chu, P. K., From Black Phosphorus to Phosphorene: Basic Solvent Exfoliation, Evolution of Raman Scattering, and Applications to Ultrafast Photonics. *Adv. Funct. Mater.* **2015,** *25* (45), 6996-7002.

8. Xing, C.; Liu, L.; Fan, D.; Peng, Z.; Zhang, H., Two-dimensional pnictogens, their chemistry and applications. *FlatChem* **2019,** *13*, 8-24.

9. Watts, M. C.; Picco, L.; Russell-Pavier, F. S.; Cullen, P. L.; Miller, T. S.; Bartuś, S. P.; Payton, O. D.; Skipper, N. T.; Tileli, V.; Howard, C. A., Production of phosphorene nanoribbons. *Nature* **2019,** *568* (7751), 216-220.

10. Zhang, S.; Guo, S.; Chen, Z.; Wang, Y.; Gao, H.; Gomez-Herrero, J.; Ares, P.; Zamora, F.; Zhu, Z.; Zeng, H., Recent progress in 2D group-VA semiconductors: from theory to experiment. *Chem. Soc. Rev.* **2018,** *47* (3), 982-1021.

11. Corbridge, D. E. C.; Lowe, E. J., Structure of White Phosphorus: Single Crystal X-Ray Examination. *Nature* **1952,** *170* (4328), 629-629.

12. Simon, A.; Borrmann, H.; Horakh, J., On the Polymorphism of White Phosphorus. *Chem. Ber.* **1997,** *130* (9), 1235-1240.

13. Hultgren, R.; Gingrich, N. S.; Warren, B. E., The Atomic Distribution in Red and Black Phosphorus and the Crystal Structure of Black Phosphorus. *J. Chem. Phys.* **1935,** *3* (6), 351-355.

14. Zaug, J. M.; Soper, A. K.; Clark, S. M., Pressure-dependent structures of amorphous red phosphorus and the origin of the first sharp diffraction peaks. *Nature Materials* **2008,** *7* (11), 890-899.

15. Ruck, M.; Hoppe, D.; Wahl, B.; Simon, P.; Wang, Y.; Seifert, G., Fibrous Red Phosphorus. *Angew. Chem. Int. Ed.* **2005,** *44* (46), 7616-7619.

16. Pfitzner, A.; Bräu, M. F.; Zweck, J.; Brunklaus, G.; Eckert, H., Phosphorus Nanorods—Two Allotropic Modifications of a Long-Known Element. *Angew. Chem. Int. Ed.* **2004,** *116* (32), 4324-4327.

17. Winchester, R. A. L.; Whitby, M.; Shaffer, M. S. P., Synthesis of Pure Phosphorus Nanostructures. *Angew. Chem. Int. Ed.* **2009,** *48* (20), 3616-3621.

18. Hittorf, W., Zur Kenntniss des Phosphors. *Ann. Phys. (Berlin)* **1865,** *202* (10), 193-228.

19. Schusteritsch, G.; Uhrin, M.; Pickard, C. J., Single-Layered Hittorf's Phosphorus: A Wide-Bandgap High Mobility 2D Material. *Nano Lett.* **2016,** *16* (5), 2975-2980.

20. Woomer, A. H.; Farnsworth, T. W.; Hu, J.; Wells, R. A.; Donley, C. L.; Warren, S. C., Phosphorene: Synthesis, Scale-Up, and Quantitative Optical Spectroscopy. *ACS Nano* **2015,** *9* (9), 8869-8884.

21. Schlesinger, M. E., The Thermodynamic Properties of Phosphorus and Solid Binary Phosphides. *Chem. Rev.* **2002,** *102* (11), 4267-4302.

22. Zhang, J. L.; Zhao, S.; Han, C.; Wang, Z.; Zhong, S.; Sun, S.; Guo, R.; Zhou, X.; Gu, C. D.; Yuan, K. D.; Li, Z.; Chen, W., Epitaxial Growth of Single Layer Blue Phosphorus: A New Phase of Two-Dimensional Phosphorus. *Nano Letters* **2016,** *16* (8), 4903-4908.

23. Han, W. H.; Kim, S.; Lee, I.-H.; Chang, K. J., Prediction of Green Phosphorus with Tunable Direct Band Gap and High Mobility. *J. Phys. Chem. Lett.* **2017,** *8* (18), 4627-4632.

24. Greaves, G. N.; Elliott, S. R.; Davis, E. A., Amorphous arsenic. *Adv. Phys.* **1979,** *28* (1), 49-141.

25. Smith, P. M.; Leadbetter, A. J.; Apling, A. J., The structures of orthorhombic and vitreous arsenic. *Philos. Mag.* **1975,** *31* (1), 57-64.

26. Krebs, H.; Steffen, R., Neubestimmung der Nahordnung im glasigen Selen, im explosiven Antimon und im β- und γ-Arsen. *Z. anorg. allg. Chem.* **1964,** *327* (3-4), 224-237.

27. Bettendorff, A., Allotropische Zustände des Arsens. *Liebigs Ann. Chem.* **1867,** *144* (1), 110-114.

28. Rodionov, A.; Kalendarev, R.; Eiduss, J., Photostimulated structural changes in yellow arsenic. *J. Phys.: Cond. Matt.* **1995,** *7* (29), 5805.

29. Bai, X.; Zhang, Q.; Gao, A.; Yang, J., Arsenic clusters Asn (n=6–16) and their anions: Structures, thermochemistry, and electron affinities. *Comput. Theor. Chem.* **2013,** *1009*, 94-102.

30. Zhang, S.; Xie, M.; Li, F.; Yan, Z.; Li, Y.; Kan, E.; Liu, W.; Chen, Z.; Zeng, H., Semiconducting Group 15 Monolayers: A Broad Range of Band Gaps and High Carrier Mobilities. *Angew. Chem. Int. Ed.* **2015,** *55* (5), 1666-1669.

31. Kamal, C.; Ezawa, M., Arsenene: Two-dimensional buckled and puckered honeycomb arsenic systems. *Phys. Rev. B* **2015,** *91* (8), 085423.

32. Sharma, S.; Kumar, S.; Schwingenschlögl, U., Arsenene and Antimonene: Two-Dimensional Materials with High Thermoelectric Figures of Merit. *Phys. Rev. Appl.* **2017,** *8* (4), 044013.

33. Tsai, H.-S.; Wang, S.-W.; Hsiao, C.-H.; Chen, C.-W.; Ouyang, H.; Chueh, Y.-L.; Kuo, H.-C.; Liang, J.-H., Direct Synthesis and Practical Bandgap Estimation of Multilayer Arsenene Nanoribbons. *Chem. Mater.* **2016,** *28* (2), 425-429.

34. Gusmao, R.; Sofer, Z.; Bousa, D.; Pumera, M., Pnictogen (As, Sb, Bi) Nanosheets for Electrochemical Applications Are Produced by Shear Exfoliation Using Kitchen Blenders. *Angewandte Chemie-International Edition* **2017,** *56* (46), 14417-14422.

35. Vishnoi, P.; Mazumder, M.; Pati, S. K.; R. Rao, C. N., Arsenene nanosheets and nanodots. *New J. Chem.* **2018,** *42* (17), 14091-14095.

36. Qi, Z.-H.; Hu, Y.; Jin, Z.; Ma, J., Tuning the liquid-phase exfoliation of arsenic nanosheets by interaction with various solvents. *Phys. Chem. Chem. Phys.* **2019,** *21* (23), 12087-12090.

37. Stock, A.; Guttmann, O., Concerning antimony hydrogen and yellow antimony. *Berichte Der Deutschen Chemischen Gesellschaft* **1904,** *37*, 885-900.

38. Rosenblatt, G. M., THE COMPOSITION OF ANTIMONY VAPOR. *J. Phys. Chem.* **1962,** *66* (11), 2259-2260.

39. Coffin, C. C.; Johnston, S., Studies on Explosive Antimony. I. The Microscopy of Polished Surfaces. *Proc. Royal Soc. Lond.* **1934,** *146* (858), 564-570.

40. Aymerich, F. M.; Delunas, A., On the explosive semiconductor-semimetal transition of antimony. *Phys. Status Solidi B* **1975,** *31* (1), 165-170.

41. Ares, P.; Aguilar-Galindo, F.; Rodríguez-San-Miguel, D.; Aldave, D. A.; Díaz-Tendero, S.; Alcamí, M.; Martín, F.; Gómez-Herrero, J.; Zamora, F., Mechanical Isolation of Highly Stable Antimonene under Ambient Conditions. *Adv. Mater.* **2016,** *28* (30), 6332-6336.

42. Gibaja, C.; Rodriguez-San-Miguel, D.; Ares, P.; Gómez-Herrero, J.; Varela, M.; Gillen, R.; Maultzsch, J.; Hauke, F.; Hirsch, A.; Abellán, G.; Zamora, F., Few-Layer Antimonene by Liquid-Phase Exfoliation. *Angew. Chem. Int. Ed.* **2016,** *55* (46), 14345-14349.

43. Shao, Y.; Liu, Z.-L.; Cheng, C.; Wu, X.; Liu, H.; Liu, C.; Wang, J.-O.; Zhu, S.-Y.; Wang, Y.-Q.; Shi, D.-X.; Ibrahim, K.; Sun, J.-T.; Wang, Y.-L.; Gao, H.-J., Epitaxial Growth of Flat Antimonene Monolayer: A New Honeycomb Analogue of Graphene. *Nano Lett.* **2018,** *18* (3), 2133-2139.

44. Wang, X.; Song, J.; Qu, J., Antimonene: From Experimental Preparation to Practical Application. *Angew. Chem. Int. Ed.* **2019,** *58* (6), 1574-1584.

45. Shi, L.; Rohringer, P.; Suenaga, K.; Niimi, Y.; Kotakoski, J.; Meyer, J. C.; Peterlik, H.; Wanko, M.; Cahangirov, S.; Rubio, A.; Lapin, Z. J.; Novotny, L.; Ayala, P.; Pichler, T.,

Confined linear carbon chains as a route to bulk carbyne. *Nat. Mater.* **2016,** *15* (6), 634-639.

46. Nakanishi, Y.; Omachi, H.; Fokina, N. A.; Schreiner, P. R.; Kitaura, R.; Dahl, J. E. P.; Carlson, R. M. K.; Shinohara, H., Template Synthesis of Linear-Chain Nanodiamonds Inside Carbon Nanotubes from Bridgehead-Halogenated Diamantane Precursors. *Angew. Chem.* **2015,** *127* (37), 10952-10956.

47. Kuzmany, H.; Shi, L.; Kurti, J.; Koltai, J.; Chuvilin, A.; Saito, T.; Pichler, T., The growth of new extended carbon nanophases from ferrocene inside single-walled carbon nanotubes. *Physica Status Solidi-Rapid Research Letters* **2017,** *11* (8), 7.

48. Fan, X.; Dickey, E. C.; Eklund, P. C.; Williams, K. A.; Grigorian, L.; Buczko, R.; Pantelides, S. T.; Pennycook, S. J., Atomic Arrangement of Iodine Atoms inside Single-Walled Carbon Nanotubes. *Phys. Rev. Lett.* **2000,** *84* (20), 4621-4624.

49. Fujimori, T.; Morelos-Gómez, A.; Zhu, Z.; Muramatsu, H.; Futamura, R.; Urita, K.; Terrones, M.; Hayashi, T.; Endo, M.; Young Hong, S.; Chul Choi, Y.; Tománek, D.; Kaneko, K., Conducting linear chains of sulphur inside carbon nanotubes. *Nat. Comm.* **2013,** *4*, 2162.

50. Fujimori, T.; dos Santos, R. B.; Hayashi, T.; Endo, M.; Kaneko, K.; Tománek, D., Formation and Properties of Selenium Double-Helices inside Double-Wall Carbon Nanotubes: Experiment and Theory. *ACS Nano* **2013,** *7* (6), 5607-5613.

51. Medeiros, P. V. C.; Marks, S.; Wynn, J. M.; Vasylenko, A.; Ramasse, Q. M.; Quigley, D.; Sloan, J.; Morris, A. J., Single-Atom Scale Structural Selectivity in Te Nanowires Encapsulated Inside Ultranarrow, Single-Walled Carbon Nanotubes. *ACS Nano* **2017,** *11* (6), 6178-6185.

52. Zhang, J.; Zhao, D.; Xiao, D.; Ma, C.; Du, H.; Li, X.; Zhang, L.; Huang, J.; Huang, H.; Jia, C.-L.; Tománek, D.; Niu, C., Assembly of Ring-Shaped Phosphorus within Carbon Nanotube Nanoreactors. *Angewandte Chemie International Edition* **2017,** *56* (7), 1850-1854.

53. Hart, M.; White, E. R.; Chen, J.; McGilvery, C. M.; Pickard, C. J.; Michaelides, A.; Sella, A.; Shaffer, M. S. P.; Salzmann, C. G., Encapsulation and Polymerization of White Phosphorus Inside Single-Wall Carbon Nanotubes. *Angew. Chem. Int. Ed.* **2017,** *56* (28), 8144-8148.

54. Hart, M.; Chen, J.; Michaelides, A.; Sella, A.; Shaffer, M. S. P.; Salzmann, C. G., One-Dimensional Arsenic Allotropes: Polymerization of Yellow Arsenic Inside Single-Wall Carbon Nanotubes. *Angew. Chem. Int. Ed.* **2018,** *57*, 11649-11653.

55. Urquhart, J., First sighting of 'pink phosphorus' caged in carbon nanotubes. *Chemistry World* **2017,** *July 2017*, 35.

56. Loiseau, A.; Pascard, H., Synthesis of long carbon nanotubes filled with Se, S, Sb and Ge by the arc method. *Chem. Phys. Lett.* **1996,** *256* (3), 246-252.

57. Tobias, G.; Shao, L.; Salzmann, C. G.; Huh, Y.; Green, M. L. H., Purification and Opening of Carbon Nanotubes Using Steam. *J. Phys. Chem. B* **2006,** *110* (45), 22318-22322.

58. Gómez-Rodríguez, A.; Beltrán-del-Río, L. M.; Herrera-Becerra, R., SimulaTEM: Multislice simulations for general objects. *Ultramicroscopy* **2010,** *110* (2), 95-104.

59. Kresse, G.; Furthmüller, J., Efficient iterative schemes for ab initio total-energy calculations using a plane-wave basis set. *Phys. Rev. B* **1996,** *54* (16), 11169-11186.

60. Kresse, G.; Joubert, D., From ultrasoft pseudopotentials to the projector augmented-wave method. *Phys. Rev. B* **1999,** *59* (3), 1758-1775.

61. Jiří, K.; David, R. B.; Angelos, M., Chemical accuracy for the van der Waals density functional. *J. Phys.: Cond. Matt.* **2010,** *22* (2), 022201.

62. Chen, J.; Schusteritsch, G.; Pickard, C. J.; Salzmann, C. G.; Michaelides, A., Two Dimensional Ice from First Principles: Structures and Phase Transitions. *Phys. Rev. Lett.* **2016,** *116* (2), 025501.

63. Bachilo, S. M.; Balzano, L.; Herrera, J. E.; Pompeo, F.; Resasco, D. E.; Weisman, R. B., Narrow (n,m)-distribution of single-walled carbon nanotubes grown using a solid supported catalyst. *J. Am. Chem. Soc.* **2003,** *125* (37), 11186-11187.

64. O'Connell, M. J.; Bachilo, S. M.; Huffman, C. B.; Moore, V. C.; Strano, M. S.; Haroz, E. H.; Rialon, K. L.; Boul, P. J.; Noon, W. H.; Kittrell, C.; Ma, J. P.; Hauge, R. H.; Weisman, R. B.; Smalley, R. E., Band gap fluorescence from individual single-walled carbon nanotubes. *Science* **2002,** *297* (5581), 593-596.

65. Clancy, A. J.; White, E. R.; Tay, H. H.; Yau, H. C.; Shaffer, M. S. P., Systematic comparison of conventional and reductive single-walled carbon nanotube purifications. *Carbon* **2016,** *108*, 423-432.

66. Seidl, M.; Balázs, G.; Scheer, M., The Chemistry of Yellow Arsenic. *Chem. Rev.* **2019**.

67. Waseda, Y.; Suzuki, K., Structure of liquid antimony by neutron diffraction. *Phys. Status Solidi B* **1971,** *47* (2), 581-590.

68. Moser, Z.; Gasior, W.; Pstrus, J.; Ishihara, S.; Liu, X. J.; Ohnuma, I.; Kainuma, R.; Ishida, K., Surface tension and density measurements of Sn-Ag-Sb liquid alloys and phase diagram calculations of the Sn-Ag-Sb ternary system. *Materials Transactions* **2004,** *45* (3), 652-660.

69. Dujardin, E.; Ebbesen, T. W.; Hiura, H.; Tanigaki, K., CAPILLARITY AND WETTING OF CARBON NANOTUBES. *Science* **1994,** *265* (5180), 1850-1852.

70. Kushvaha, S. S.; Yan, Z.; Xiao, W.; Wang, X. S., Surface morphology of crystalline antimony islands on graphite at room temperature. *J. Phys. Condens. Matter* **2006,** *18* (13), 3425-3434.

71. Hart, M. Filling single-walled carbon nanotubes with highly reactive chemicals. PhD thesis, University College London, London, UK, 2019.

72. Schwarzmaier, C.; Schindler, A.; Heindl, C.; Scheuermayer, S.; Peresypkina, E. V.; Virovets, A. V.; Neumeier, M.; Gschwind, R.; Scheer, M., Stabilization of Tetrahedral P4 and As4 Molecules as Guests in Polymeric and Spherical Environments. *Angew. Chem. Int. Ed.* **2013,** *52* (41), 10896-10899.

73. Seitz, A. E.; Hippauf, F.; Kremer, W.; Kaskel, S.; Scheer, M., Facile storage and release of white phosphorus and yellow arsenic. *Nature Commun.* **2018,** *9* (1), 361.

74. Spitzer, F.; Sierka, M.; Latronico, M.; Mastrorilli, P.; Virovets, A. V.; Scheer, M., Fixation and Release of Intact E-4 Tetrahedra (E = P, As). *Angew. Chem. Int. Ed.* **2015,** *54* (14), 4392-4396.

75. Ersan, F.; Aktürk, E.; Ciraci, S., Stable, one-dimensional suspended and supported monatomic chains of pnictogens: a metal–insulator framework. *Phys. Chem. Chem. Phys.* **2019,** *21* (27), 14832-14845.

76. Hart, M.; Chen, J.; Michaelides, A.; Sella, A.; Shaffer, M. S. P.; Salzmann, C. G. One-Dimensional Pnictogen Allotropes Inside Single-Wall Carbon Nanotubes. 2019, DOI: 10.26434/chemrxiv.8959538.v1. ChemRxiv e-Print archive. https://chemrxiv.org/articles/One-Dimensional_Pnictogen_Allotropes_Inside_Single-Wall_Carbon_Nanotubes/8959538/1 (accessed Oct 22, 2019).

SYNOPSIS

One-dimensional pnictogen allotropes inside carbon nanotubes are investigated in detail. In addition to the first observations of double-stranded phosphorus and antimony zig-zag ladders, the diameter of the confinement as well as the filling conditions are shown to impact on the yields of the various pnictogen nanostructures. Computational calculations help rationalizing the observed filling yields and predict a wide range of electronic properties of the encapsulated pnictogens from insulating to fully metallic.

For Table of Contents Only